NEOPLASIA
www.neoplasia.com

Volume 13 Number 6 June 2011 pp. 516–525 **516**

Targeting of α_v-Integrins in Stem/Progenitor Cells and Supportive Microenvironment Impairs Bone Metastasis in Human Prostate Cancer[1,2]

Geertje van der Horst*, Christel van den Hoogen*, Jeroen T. Buijs*, Henry Cheung*, Henny Bloys†, Rob C.M. Pelger*, Giocondo Lorenzon‡, Bertrand Heckmann‡, Jean Feyen‡, Philippe Pujuguet‡, Roland Blanque‡, Philippe Clément-Lacroix‡ and Gabri van der Pluijm*,†

*Department of Urology, Leiden University Medical Centre, Leiden, The Netherlands; †Department of Endocrinology, Leiden University Medical Centre, Leiden, The Netherlands; ‡Galapagos SASU, Romainville, France

Abstract

Acquisition of an invasive phenotype by cancer cells is a requirement for bone metastasis. Transformed epithelial cells can switch to a motile, mesenchymal phenotype by epithelial-mesenchymal transition (EMT). Recently, it has been shown that EMT is functionally linked to prostate cancer stem cells, which are not only critically involved in prostate cancer maintenance but also in bone metastasis. We showed that treatment with the nonpeptide α_v-integrin antagonist GLPG0187 dose-dependently increased the E-cadherin/vimentin ratio, rendering the cells a more epithelial, sessile phenotype. In addition, GLPG0187 dose-dependently diminished the size of the aldehyde dehydrogenase high subpopulation of prostate cancer cells, suggesting that α_v-integrin plays an important role in maintaining the prostate cancer stem/progenitor pool. Our data show that GLPG0187 is a potent inhibitor of osteoclastic bone resorption and angiogenesis *in vitro* and *in vivo*. Real-time bioluminescent imaging in preclinical models of prostate cancer demonstrated that blocking α_v-integrins by GLPG0187 markedly reduced their metastatic tumor growth according to *preventive* and *curative* protocols. Bone tumor burden was significantly lower in the *preventive* protocol. In addition, the number of bone metastases/mouse was significantly inhibited. In the *curative* protocol, the progression of bone metastases and the formation of new bone metastases during the treatment period was significantly inhibited. In conclusion, we demonstrate that targeting of integrins by GLPG0187 can inhibit the *de novo* formation and progression of bone metastases in prostate cancer by antitumor (including inhibition of EMT and the size of the prostate cancer stem cell population), antiresorptive, and antiangiogenic mechanisms.

Neoplasia (2011) 13, 516–525

Introduction

Prostate cancer is the most commonly diagnosed malignancy in many western countries and the second leading cause of cancer death in male [1]. Because of the progress made in the diagnosis and treatment of primary prostate cancer, mortality in 70% to 80% of the patients is increasingly linked to metastatic disease, often occult at time of diagnosis or surgery. The bone marrow is the most frequent metastatic site for prostate cancer, and colonization of bone marrow is a critical step in the formation of these bone metastases.

Acquisition of an invasive phenotype of cancer cells in the primary tumor is a requirement for bone metastasis. Transformed epithelial cells

Address all correspondence to: Dr. Gabri van der Pluijm, Department of Urology J3-100, Leiden University Medical Center, Albinusdreef 2, 2333 ZA Leiden, The Netherlands. E-mail: G.van_der_Pluijm@lumc.nl

[1]This work was supported by the European Sixth Framework Programs PRIMA and PROMET and financial support from Galapagos.

[2]This article refers to supplementary materials, which are designated by Table W1 and Figures W1 to W5 and are available online at www.neoplasia.com.

Received 7 January 2011; Revised 29 March 2011; Accepted 4 April 2011

DOI 10.1593/neo.11122

can switch from a sessile, epithelial to a motile, mesenchymal phenotype by epithelial-mesenchymal transition (EMT) [2]. It has been shown that EMT may generate cells with properties of stem cells in human breast and prostate cancer [2,3].

Recently, we found that stem/progenitor cells, besides their role in tumorigenicity, are highly migratory cells that are involved in bone metastasis formation [4,5]. Micrometastases are initially formed in perivascular niches of the bone marrow sinusoids (unpublished observations). Subsequent outgrowth to clinically overt bone metastases requires multiple tumor-stroma interactions including angiogenesis and bone resorption [6,7]. Despite the predominant osteoblastic phenotype of bone metastases from prostate cancer, tumor-induced osteoclastic bone destruction is strongly elevated. A multitude of these functions, including bone homing by cancer cells, tumor-induced angiogenesis, and osteoclastic bone resorption, are dependent on adhesion receptors of the integrin family, particularly α_v-integrins [8–10]. Integrins are cell surface receptors for extracellular matrix proteins that play a key role in a variety of biologic activities including signal transduction, cell adhesion, cell survival, proliferation, migration angiogenesis, and gene expression [6,11–13]. Integrins are heterodimers consisting of an α- and β-subunit, each combination having its own binding specificity and signaling properties.

Prostate cancer growth is correlated with specific expression and deregulation of several integrin subunits [6,14–17]. The expression of $\alpha_v\beta_3$ integrin in advanced prostate cancer is upregulated compared to normal prostate tissue, and prostate cancer cells contain a functional $\alpha_v\beta_3$ integrin [18,19]. As we have recently shown, the expression of α_v-integrin is upregulated in human prostate cancer cells with tumor- and metastasis-initiating properties [4]. In addition, α_v-integrins are upregulated in a prostate cancer stem cell population ($CD133^+$, $CD44^+$, and $\alpha_2\beta_1^{hi}$) compared with the committed progenitor subpopulation [20].

Previous studies using RGD recognition (i.e., using RGD peptides), inhibitory antibodies, or siRNA to block integrins have shown encouraging results [21–23]. For example, administration of human α_v-siRNA significantly inhibited the growth of human prostate cancer xenografts in bone and increased apoptosis of the tumor cells [23]. Expression of a fully functional $\alpha_v\beta_3$ integrin enabled tumor growth in bone, whereas inactive or constitutively active mutants did not [24]. These data suggest that $\alpha_v\beta_3$ integrin modulates prostate cancer growth in bone.

In addition, α_v as well as α_5-integrins play a pivotal role in the supportive stroma in bone metastasis, particularly in tumor-induced osteoclastic bone resorption and angiogenesis [10,25–29]. For example, Mahabeleshwar et al. [30] showed that vascular endothelial growth factor–stimulated angiogenesis is reduced in β_3-deficient mice compared to wild type, which resulted in smaller prostate tumors. Antiangiogenic agents such as JF-10-81, a camptothecin conjugate, reduced the expression of $\alpha_v\beta_3$ and $\alpha_v\beta_5$ in PC3 cells and blocked tumor cell adhesion and angiogenesis *in vivo* [31]. Treatment of PC-3 xenografts with an RGD mimetic (S247) resulted in both antitumor and antiangiogenic effects. Combination with radiation significantly augmented these effects compared to either therapy alone [32].

Taken together, inhibiting α_v-integrin function seems a promising strategy to prevent prostate cancer progression at various stages.

In this article, we evaluated the efficacy of GLPG0187, a nonpeptide RGD antagonist on prostate cancer growth in preclinical models of prostate cancer metastasis. We demonstrate that targeting of the $\alpha_v\beta_3$ integrins by GLPG0187 can inhibit both *de novo* formation as well as progression of bone metastases in prostate cancer.

Materials and Methods

Cell Culture

Human prostate cancer PC-3M-Pro4/luc$^+$ cells were maintained in Dulbecco modified Eagle medium (GibcoBRL, Breda, The Netherlands) containing 4.5 g glucose/L supplemented with 10% FCII, 100 U/ml penicillin, 50 μg/ml streptomycin, and 800 μg/ml geneticin/G418 (Invitrogen, Breda, The Netherlands) as described previously [33] (see Supplementary Methods). Cells were regularly monitored and were certified free of mycoplasma contamination.

Osteoclastogenesis Assay

Murine bone marrow cells were cultured in α-minimum essential medium containing 10% heat-inactivated fetal bovine serum in the presence of RANKL (PeproTech, Neuilly-sur Seine, France; 6 ng/ml) and membrane form of macrophage colony-stimulating factor (R&D Systems, Oxford, UK; 25 ng/ml) in 96-well tissue culture plates [34]. Cells were fixed and stained for tartrate-resistant acid phosphatase (TRAcP) activity after 5 days in culture, using a commercial kit (387-A; Sigma-Aldrich, St Louis, MO).

Migration Assay

Migration was performed in 8-μm Transwell migration chambers (Costar, Amsterdam, The Netherlands). A total of 6×10^4 prestarved (0.1% fetal calf serum) PC-3M-Pro4/luc cells were seeded in the upper chamber containing either vehicle or GLPG0187 compound and allowed to migrate toward serum-containing medium in the lower chamber. Cells were fixed after 6 hours with 4% paraformaldehyde and stained with 0.1% crystal violet (2 mg/ml; Sigma-Aldrich, The Netherlands). Three random fields were counted for each well, and mean numbers of migrated cells/field were calculated [35].

Fluorescence-Activated Cell Sorter

PC-3M-Pro4/luc cells were harvested and labeled with E-cadherin–FITC (BD Biosciences 1:10 in FACS buffer: PBS with 0.1% sodium azide and 1% fetal calf serum) for 30 minutes at 4°C in the dark. Then, cells were washed with 1 ml of FACS buffer and fixed with freshly prepared 2% formaldehyde for 15 minutes. Cells were washed with ice-cold PBS and subsequently incubated for 30 minutes at 4°C in the dark with vimentin rabbit polyclonal antibody (1:200 in FACS buffer; AbCaM, Cambridge, UK). Cells were washed twice with 1 ml of FACS buffer and incubated with goat–anti rabbit IgG-APC (Invitrogen). After washing, samples were analyzed using the Becton Dickinson FACSCalibur2 (Breda, The Netherlands) and FCS express software (De Novo Software, Los Angeles, CA). Aldehyde dehydrogenase (ALDH) activity was measured as described earlier [4].

RNA Isolation and Real-time Quantitative Polymerase Chain Reaction

RNA was extracted using TRIzol (Invitrogen) according to the manufacturer's instructions. Real-time quantitative polymerase chain reaction (qPCR) was run and analyzed with a Bio-Rad iQ5 Cycler (Bio-Rad, Veenendaal, The Netherlands). For primer sequences, see Table W1. Gene expression was measured relative to *GAPDH* expression using the following formula: $\log 2^{-\Delta\Delta Ct}$ [36].

Angiogenesis Assays

Metatarsal angiogenesis assay. Seventeen-day-old fetuses were removed from pregnant Swiss albino mice, and metatarsals were dissected as described previously [37]. The isolated metatarsals were cultured for 10 days in 24-well plates in the presence of vehicle (1:1 dimethyl sulfoxide/PBS) or different concentrations of GLPG0187. Subsequently, the metatarsals were fixed and stained for platelet/endothelial cell adhesion molecule 1 (CD31) as described previously [37]. The experiment was performed three times with eight cultures per condition.

Neonatal Tail Angiogenesis Assay

The neonatal mouse tail provides a suitable model to simultaneously assess bone angiogenesis and osteoclastogenesis *in vivo* [37]. Two-day-old neonatal Swiss albino mice were subcutaneously treated with GLPG0187 (30 mg/kg per day) or vehicle (1:1 dimethyl sulfoxide in PBS) for four consecutive days, starting at the second day after birth ($n = 4$). After 4 days of treatment the animals were killed, and the tails were stained for lectin and for osteoclasts (TRAcP staining) [37].

Xenograft Experiments

Mouse strain. Male nude mice (BALB/c *nu/nu*; Charles River, L'Arbresle, France) were housed in individual ventilated cages under sterile condition according to the Dutch guidelines for the care and use of laboratory animals (DEC 4077). Before surgical and analytical procedures were performed, the mice were anesthetized.

Intracardiac inoculation of PC-3M-Pro4/luc cells to induce systemic metastases. A single-cell suspension of 1×10^5 PC-3M-Pro4/luc cells/100 μl PBS was injected into the left cardiac ventricle of 4-week-old nude mice as described previously [33]. The progression of cancer cell growth was monitored weekly by bioluminescent imaging (BLI) using the IVIS100 Imaging System (Caliper LifeSciences, Hopkinton, MA) [33]. Analyses for each metastatic site were performed after definition of the region of interest and quantified with Living Image (Caliper LifeSciences). Values are expressed as relative light units.

Histomorphometry, histochemistry, and immunohistochemistry. Dissected tissues from animal studies were fixed in 4% paraformaldehyde (pH 6.8), decalcified (only bones) as described previously and processed for paraffin embedding, sectioning, and staining [4,37].

Statistical Analysis

Data are presented as mean ± SEM. Two-way analysis of variance was performed followed by the *post hoc* Bonferroni test. $P < .05$ was considered to be significant ($^*P < .05$, $^{**}P < .01$, $^{***}P < .001$).

Results

GLPG0187 and Cellular Characteristics of PC-3M-Pro4 Prostate Cancer Cells

Bone homing of cancer cells, tumor-induced angiogenesis, and osteoclastic bone resorption are dependent on adhesion receptors of the integrin family, particularly α_v-integrins. Tumor-initiating cells have recently been identified in many solid tumors, including breast and prostate. Evidence is mounting that tumor-initiating cells are not only critically involved in cancer initiation and progression but also in colonization and bone metastasis formation [4,5,38–40]. Strikingly, α_v-integrin expression is associated with the basal layer of the human prostate and its expression is also upregulated in tumor-initiating cells (Figure W1*A*; source: www.proteinatlas.org) [4,20]. The prostate cancer cell line PC-3 and its derivative PC-3M-Pro4/luc displayed high levels of α_v-integrin as detected by immunohistochemistry and flow cytometry (99.7% of the cells express α_v-integrin; Figure W1, *A* and *B*). Furthermore, α_v integrins are highly expressed in osteoclasts and activated endothelial cells where they play functional roles related to bone resorption and angiogenesis, respectively [41,42].

In the present study, we investigated the effects of blocking α_v-integrin on prostate cancer growth and bone metastasis. The nonpeptide RGD integrin receptor antagonist, GLPG0187, blocks six integrin receptors and displays a unique anti-integrin profile in solid-phase integrin-ligand binding assays (see Supplementary Methods). In a solid-phase assay, GLPG0187 showed selectivity for several RGD integrin receptors with the following IC_{50}: 1.3 nM for $\alpha_V\beta_1$, 3.7 nM for $\alpha_V\beta_3$, 2.0 nM for $\alpha_V\beta_5$, 1.4 nM for $\alpha_V\beta_6$, 1.2 nM for $\alpha_V\beta_8$, and 7.7 nM for $\alpha_5\beta_1$. It is important to note that GLPG0187 has poor affinity ($IC_{50} > 10$ μM) for the platelet-specific integrin receptor integrin-$\alpha_{II}\beta$ [43].

Effect of GLPG0187 on Osteoclastogenesis In Vitro *and* In Vivo

To determine whether GLPG0187 displayed effects on the supportive tumor stroma, first the effects of GLPG0187 on osteoclastogenesis were assessed (schematic representation; Figure 1*A*) [44].

During osteoclast differentiation, podosomes are found as components of larger structures known as clusters, rings, or belts. As shown in Figure 1*B*, osteoclasts can be subdivided into three different categories: moving, sitting, and rings according to their morphology (shown by light microscopy and actin staining). GLPG0187 significantly decreased the amount of osteoclasts forming a ring, a structure necessary for osteoclastic resorption (Figure 1*C*).

Osteoclastogenesis induced by RANKL and mM-CSF from mice bone marrow osteoclast precursors was inhibited by GLPG0187 (0.39–200 nM), with a statistically significant effect at concentrations ≥3 nM (Figure 1*D*).

In orchidectomized (ORX) rodents, increased bone resorption due to an imbalance in osteoblastic and osteoclastic activity, results in a significantly reduced trabecular bone volume (BV/TV) and bone mineral density (BMD) in the proximal tibia metaphysis.

ORX mice were treated with GLPG0187, immediately after castration, either by subcutaneous route at the doses of 10, 30, or 100 mg/kg (twice a day) or orally at the doses of 30, 100, or 300 mg/kg (twice a day). In line with the efficacy of GLPG0187 to inhibit osteoclast formation and osteoclastic bone resorption, with either route of administration, GLPG0187 significantly and dose-dependently prevented ORX-induced bone loss (Figure W2).

Effect of GLPG0187 on Angiogenesis In Vitro *and* In Vivo

Subsequently, the effect of GLPG0187 on angiogenesis was evaluated using *in vitro* and *in vivo* models [37]. Continuous treatment of 17-day-old fetal murine metatarsals for 10 days with various doses

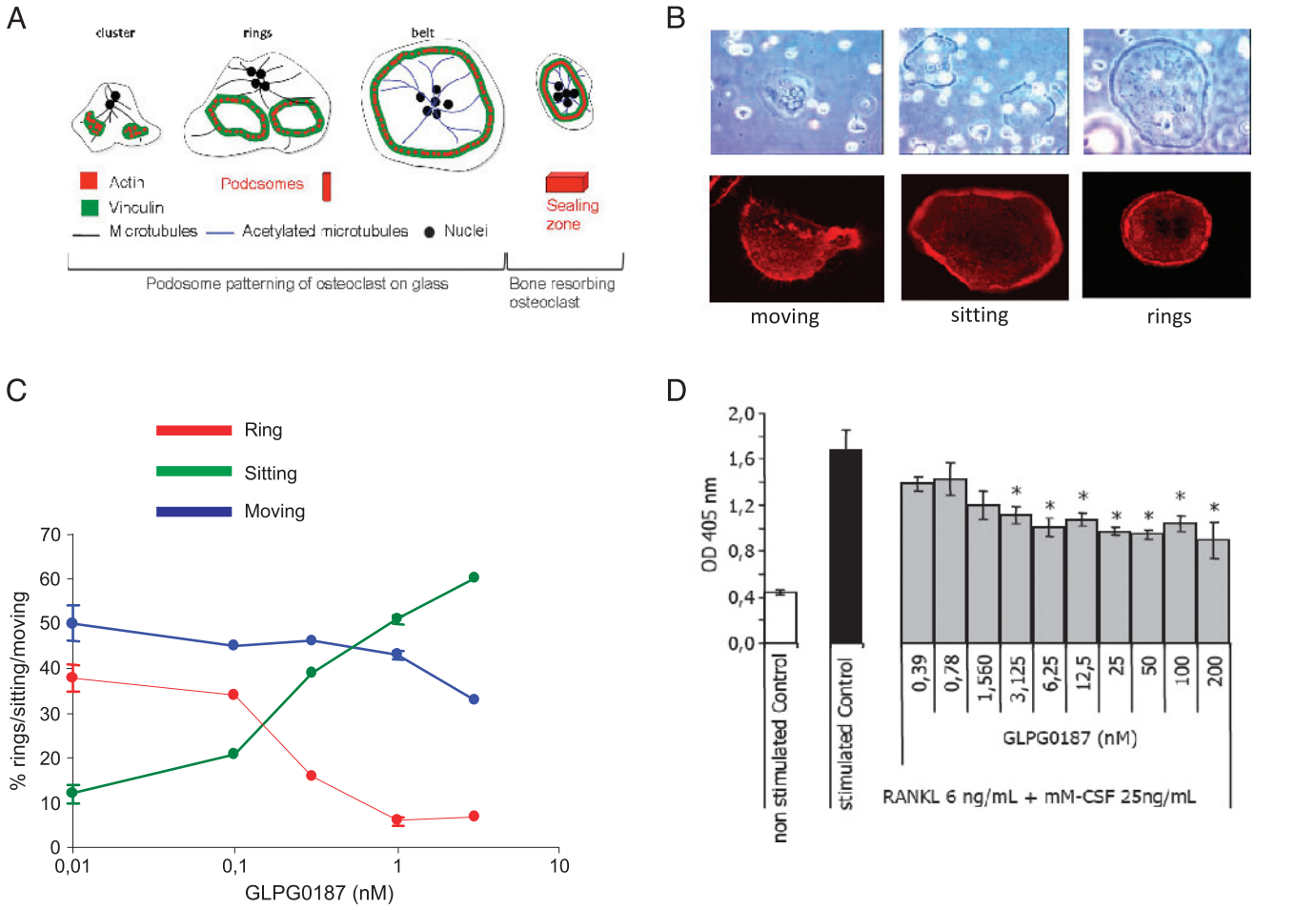

Figure 1. GLPG0187 affects osteoclastogenesis. (A) Schematic representation of osteoclast formation in an osteoclast model adapted from Jurdic et al. [44]. (B) Representative images of light microscopy and fluorescent actin staining showing the different morphology of differentiating osteoclasts. (C) Effect of GLPG0187 on the amount of osteoclasts in each differentiation morphology. (D) Bone marrow cells isolated from 8-week-old female mice tibiae and femora were cultured during 5 days in the presence of RANKL and mM-CSF and of various concentrations of GLPG0187. TRAcP activity was measured using densitometry. Data are expressed as mean ± SEM ($n = 4$). *$P < .05$ *versus* stimulated control.

of GLPG0187 prevented the outgrowth of CD31-positive capillary structures in a dose-dependent manner (Figure 2, *A* and *B*).

Next, we evaluated the effects of GLPG0187 in an *in vivo* model of endochondral bone formation that can be exploited to simultaneously assess the formation of capillaries and osteoclasts. At the start of the experiment (day 2 postpartum), the 28 caudal vertebrae of the mouse-tail encompass different developmental regions [37]. From proximal to distal, vertebrae are composed of developing trabecular bone with a primitive bone marrow cavity (vertebrae 1-10), calcified avascular cartilage (vertebrae 11-21), and nonmineralized avascular cartilage (vertebrae 22-28). The invasion front was determined as the first sign of vascular invasion and/or osteoclast invasion of a developing caudal vertebra (Figure 2*C*). After 4 days of vehicle treatment, the invasion front progressed to the distal end and was located at approximately vertebra 20 (Figure 2*C*). In line with our *in vitro* observations, administration of GLPG0187 resulted in a significant delay in both invasion of the caudal vertebrae by osteoclasts and blood vessels (at V20 [capillaries] and V21 [osteoclasts], respectively, under control conditions and at V14 [capillaries] and V15 [osteoclasts], respectively, in the GLPG0187-treated animals) (Figure 2, *E–G*). Taken together, our data show that GLPG0187 is a potent inhibitor of angiogenesis both *in vitro* and *in vivo*.

Direct Effects on Tumor Cells of GLPG0187

In addition to the effects on the supportive stroma, we investigated whether GLPG0187 displayed direct effects on the tumor cells. Treatment of PC-3M-Pro4/luc prostate cancer cells with GLPG0187 resulted in a dose-dependent decrease in adhesion to tissue culture plastic as prostate cancer cells started to grow in suspension from 4 hours onward (the effect after 24 hours of treatment with GLPG0187 is seen in Figure W3*A*). This was not due to the altered viability of the treated PC-3M-Pro4/luc cells because no significant differences in cell death were found with an annexin V/PI apoptosis assay (Figure W3*B*). Moreover, the proliferation rate of PC-3M-Pro4/luc cells after 48 and 72 hours of treatment was significantly decreased (Figure W3*C*).

Acquisition of an invasive phenotype is a requirement for bone metastasis; transformed epithelial cells can switch to a motile, mesenchymal phenotype by EMT. GLPG0187 dose-dependently and significantly increased the E-cadherin/vimentin ratio in PC-3M-Pro4/luc cells, indicative of a less invasive and more epithelial phenotype (Figure 3*A*). On

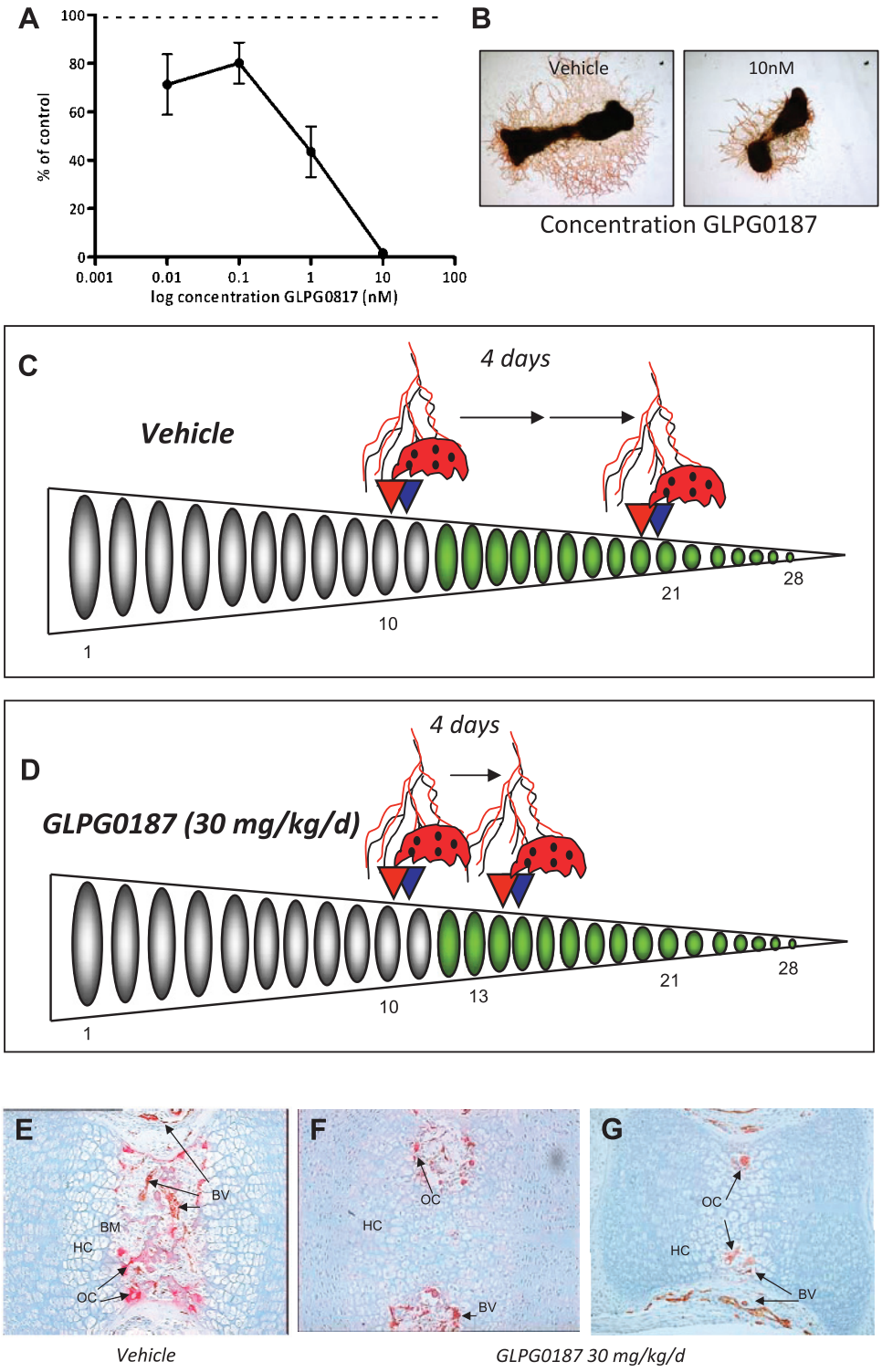

Figure 2. GLPG0187 inhibits angiogenesis both *in vitro* and *in vivo*. (A) Total area of CD31-positive capillary-like structures was determined by computerized image analysis in 17-day-old fetal mouse metatarsals treated for 10 days with either vehicle or GLPG0187. Data are expressed as percent of control ± SEM. (B) Representative images of control and 10 nM GLPG0187-treated metatarsals. Schematic representation of angiogenesis and accession to calcified cartilage of osteoclasts (adhesion to bone, migration on bone surface, and bone resorption) in the caudal vertebrae in neonatal mouse-tails under control conditions (vehicle) (C) or GLPG0187-treated conditions (D). Tails were processed and double-stained for TRAcP (red) and lectin (brown). At day 2 postpartum (p.p.), osteoclast-precursors and blood capillaries have started to invade the bone collar at caudal vertebrae 11 and 10, respectively. Four days later, osteoclast-precursors and capillaries have progressed in a distal manner, and their invasion fronts can now be identified at V20 (capillaries) and V21 (osteoclasts) under control conditions and at V14 (capillaries) and V15 (osteoclasts) in the GLPG0187-treated animals. $n = 4$ mice/group. Representative images of vertebrae 13 of vehicle treated (E) or GLPG0187-treated animals (F and G) are shown. BM indicates bone marrow; BV, blood vessels; HC, calcified cartilage; OC, osteoclast.

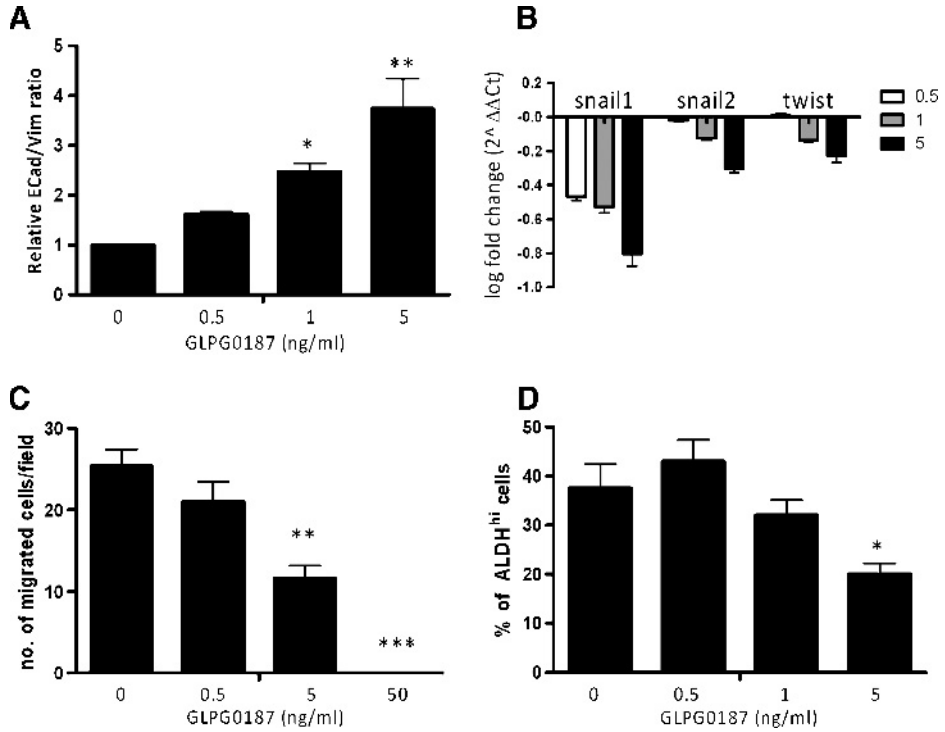

Figure 3. Effect of GLPG0187 on EMT, migration, and percentage of ALDH^{hi} stem/progenitor cells. Cells were treated for 48 hours with a concentration range of GLPG0187, and subsequently, relative E-cadherin/vimentin ratio (A) was measured with flow cytometry and levels of EMT inducers including *Snail1* and *2* and *Twist* were measured with real time qPCR (B). Data are represented as log fold change (log2$^{-\Delta\Delta Ct}$). Mean numbers of migrated PC-3M-Pro4/luc cells per field were measured (C). Data are presented as mean ± SEM (*$P <$ .05) and are representative for three independent experiments. Percentage of PC-3M-Pro4/luc cells with high ALDH activity as measured with ALDEFLUOR assay (D) [4].

treatment, the messenger RNA levels of the prometastatic regulators *Twist*, *Snail1*, and *Snail2* decreased as measured with real-time qPCR (Figure 3*B*).

Migration of PC-3M-Pro4/luc cells in a Transwell Boyden chamber was significantly and dose-dependently blocked by GLPG0187 (Figure 3*C*).

Recently, our group showed that high aldehyde dehydrogenase (ALDH^{hi}) activity can be used to identify prostate cancer cells with tumor-initiating and metastasis-initiating ability [4]. When treated with GLPG0187, the size of the ALDH^{hi} cells' subpopulation of cancer stem/progenitor cells decreased significantly (Figure 3*D*).

Treatment of human C4-2B prostate cancer cells with GLPG0187 revealed similar effects, that is, dose-dependent loss of adhesion to tissue culture plastic (Figure W5*A*) and dose-dependently increased E-cadherin/vimentin ratio (Figure W5*B*). In addition, GLPG0187 dose-dependently diminished the size of the ALDH^{hi} subpopulation of prostate cancer cells (Figure W5*C*). Migration of C4-2B cells was also dose-dependently decreased by GLPG0187 (Figure W5*D*).

Taken together, these data show that GLPG0187 dose-dependently inhibits EMT and migration and decreases the percentage of prostate cancer cells with tumor-initiating and metastasis-initiating ability.

GLPG0187 and Prostate Cancer Bone Metastasis

Subsequently, we investigated whether blocking α_v-integrin can be used to treat experimentally induced bone metastasis from human prostate cancer cells (PC-3M-Pro4/luc) according to a *preventive* protocol using bioluminescent imaging (Figure 4*A*). Total tumor burden was significantly and dose-dependently decreased in mice subcutaneously treated with GLPG0187 (Figure 4, *B-D*). Bone tumor burden was approximately 1000 times lower in the 100-mg/kg per day GLPG0187 group *versus* vehicle in the *preventive* protocol (Figure 4*E*). In addition, the number of bone metastases/mouse was significantly inhibited (Figure 4*F*).

In the *curative* protocol, bone metastases were allowed to develop for 21 days (Figure 5*A*). Subsequently, the mice were treated with an oral dosage of either vehicle or GLPG0187 (30 or 100 mg/kg per day) to investigate whether blocking α_v-integrin can be used to treat already-existing bone metastases. Total tumor burden was significantly decreased after 15 days of treatment with 30-mg/kg per day GLPG0187 (Figure 5, *B* and *C*). In addition, the progression of bone metastases was significantly inhibited on treatment from 12 days onward with both the 30- and 100-mg/kg per day GLPG0187 groups (Figure 5*D*). Importantly, the formation of new bone metastases during the treatment period was strongly inhibited in both 30- and 100-mg/kg per day GLPG0187 groups (Figure 5*E*). Similar data were obtained in another curative protocol using twice-daily subcutaneous administration of GLPG0187 (Figure W4). GLPG0187 showed significant and dose-dependent bone-sparing effects comparable to the bisphosphonate zolendronate as shown in Figure 5*F*.

Discussion

The bone marrow is the most frequent metastatic site for prostate cancer, and colonization of the bone marrow is a critical step in the formation of bone metastasis.

Integrins mediate several important processes including tumor-induced angiogenesis, tumor-induced osteoclastic bone resorption, cancer cell invasiveness, thus providing the rationale for the use of integrin inhibitors in metastatic bone disease [8–10].

It has been shown previously that $\alpha_v\beta_3$ integrin plays a crucial role in the osteotropism of various carcinomas [24,45,46]. These data have identified $\alpha_v\beta_3$ integrin as a potential therapeutic target for the treatment of bone metastases.

Acquisition of an invasive phenotype is a critical step in the formation of bone metastases. Transformed sessile, epithelial cells can switch to a motile mesenchymal phenotype by the process of EMT. During EMT, epithelial characteristics are shed, and cancer cells acquire a more mesenchymal motile cell phenotype, coinciding with increased α_v integrin expression [2]. We show that administration of GLPG0187 significantly and dose-dependently decreased adhesion and the migratory ability of human prostate cancer cells *in vitro*. In addition, treatment with an α_v inhibitor dose-dependently induced a more sessile epithelial phenotype as observed by increased E-cadherin/vimentin ratios. These data are further substantiated by a dose-dependent decrease in the expression of E-cadherin suppressors *Snail1*, *Snail2* (formerly known as *Slug*), and *Twist* [47].

Transforming growth factor β (TGFβ) is a major EMT effector in transformed cells and is a key factor in tumor progression and bone metastasis [48]. Interestingly, extensive crosstalk exists between integrins and TGFβ. TGFβ is secreted in an inactive, latent form in a complex with TGFβ latent binding proteins [49]. Dissociation of the complex by binding of integrins to the RGD motif in the TGFβ latent binding protein can activate TGFβ. In addition, TGFβ can induce the expression of several integrins, thereby enhancing the migratory and invasive behavior of cancer cells [49]. Interfering with the self-amplifying, TGFβ-driven tumor-stroma interactions, critical for tumor invasiveness and metastasis, therefore provides the rationale for the use of α_v antagonists. Interestingly, it has been shown that TGFβ plays a key role in the formation of the mammary epithelial stem cell pool in breast cancer, mediated by EMT [39,40]. Furthermore, recent evidence suggests that EMT is mechanistically

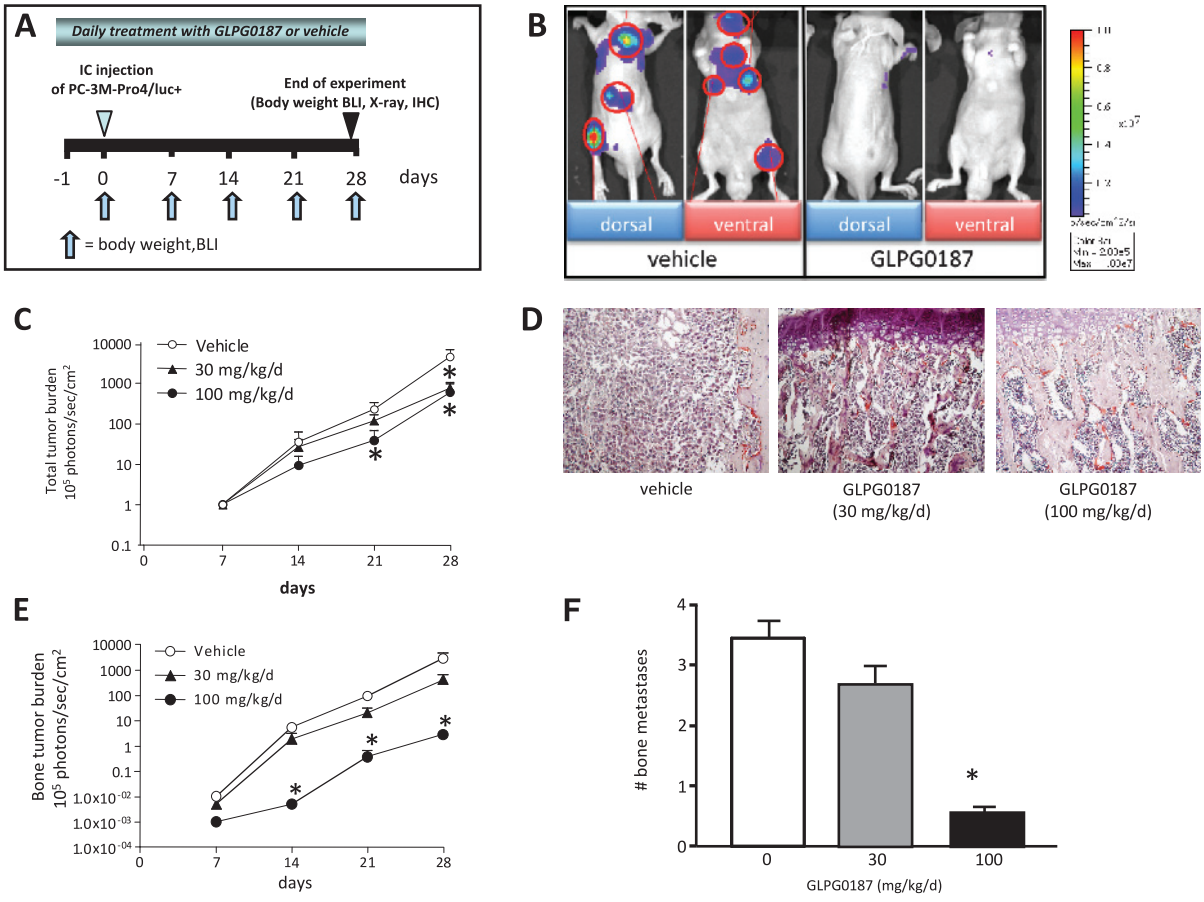

Figure 4. Effects of systemic administration of GLPG0187 on tumor growth and formation of *de novo* metastases. (A) Schematic representation of the preventive protocol. Mice were treated daily with either subcutaneously administrated vehicle or GLPG0187 from day −1 onward. At day 0, 100,000 PC-3M-Pro4/luc cells were inoculated into the left heart ventricle, and once a week, body weight was measured and BLI images were taken. (B) Representative images of mice treated with vehicle or 100 mg/kg per day GLPG0187 taken at day 28 after inoculation. (C) Total tumor burden for the mice treated with 30 mg/kg per day GLPG0187 (closed triangles), 100 mg/kg per day GLPG0187 (closed circles), or vehicle (open circles). (D) Dose-dependent reduction in tumor volume in GLPG0187-treated animals as shown by hematoxylin and eosin staining (bone images of vehicle, 30-mg/kg per day, and 100-mg/kg per day GLPG0187-treated animals, respectively). (E) Bone tumor burden for the mice treated with 30-mg/kg per day GLPG0187 (closed triangles), 100-mg/kg per day GLPG0187 (closed circles), or vehicle (open circles). (F) Total number of bone metastases per mouse (n = 10/group; *$P < .05$).

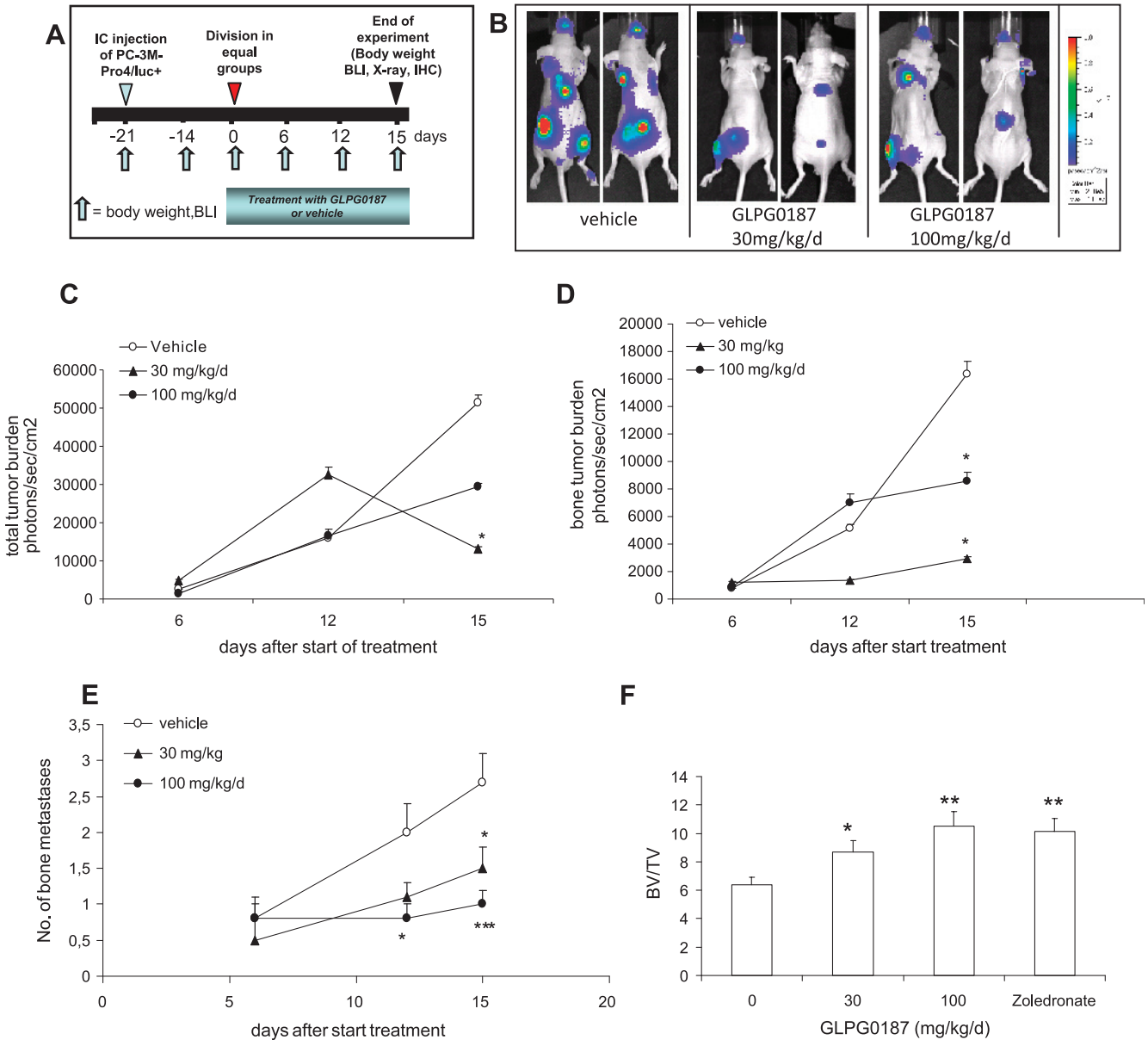

Figure 5. Effects of systemic administration (orally) of GLPG0187 on tumor growth of established bone metastases. (A) Schematic representation of the curative protocol. At day −21, 100,000 PC-3M-Pro4/luc cells were injected into the left heart ventricle, and once a week, body weight was measured, and BLI images were taken. At day 0, mice were divided into groups with equal total tumor burden. Mice were daily treated with an oral dosage of either vehicle or GLPG0187 from day 0 onward. (B) Representative images of mice treated with vehicle or 30-mg/kg per day GLPG0187 taken at day 15 after start of treatment. (C) Total tumor burden for the mice treated with 30-mg/kg per day GLPG0187 (closed triangles), 100-mg/kg per day GLPG0187 (closed circles), or vehicle (open circles). (D) Bone tumor burden for the mice treated with 30-mg/kg per day GLPG0187 (closed triangles), 100-mg/kg per day GLPG0187 (closed circles), or vehicle (open circles). (E) Total number of bone metastases per mouse (n = 10/group; *P < .05). (F) Ratio of bone volume (BV) over total volume (TV) of mice injected with either vehicle, GLPG0187, or zoledronate (10 μg/kg per day) at day 15 after start of treatment as measured with micro-CT scanning (Micro-densitometer Scanco μCT20).

linked to the formation of highly tumorigenic prostate cancer stem/progenitor cells with a mesenchymal, migratory, clonogenic phenotype [3]. EMT may therefore generate cells with properties of stem cells, which are critically involved not only in tumor initiation and progression but also in colonization and bone metastasis formation [3–5,38–40]. Recently, we found that ALDH^{hi} activity can be used to identify prostate cancer cells with increased tumor-initiating and metastasis-initiating ability [4]. Interestingly, the level of α_v-integrin was significantly increased in ALDH^{hi} cancer cells compared to the ALDH^{low} prostate cancer cells [4]. Inhibiting α_v-integrin with GLPG0187 dose-dependently inhibited the percentage of ALDH^{hi} cells in prostate cancer cell lines, suggesting that α_v-integrin plays an important role in maintaining the prostate cancer stem/progenitor pool. Our observations are in line with data showing a high expression of α_v-integrin in the prostate basal layer compared to more differentiated counterparts [20].

Besides the direct effects of inhibiting α_v-integrin on the tumor cells, GLPG0187 also affected the tumor microenvironment, in particular angiogenesis and osteoclastic bone resorption. Similar to

invasive cancer cells, activated endothelial cells depend on α_v integrins for *de novo* formation of capillaries from preexisting blood vessels. GLPG0187 significantly and dose-dependently inhibited angiogenesis both in *in vitro* and *in vivo* angiogenesis assays.

Administration of GLPG0187 reduced osteoclastogenesis and bone resorption both *in vitro* and *in vivo*. The levels of inhibition were comparable to the bisphosphonate zolendronate [41].

In a preventive study, GLPG0187 could inhibit bone metastases formation and dose-dependently inhibited tumor burden. Moreover, oral or subcutaneous administration of GLPG0187 could block the progression of already existing bone metastases and prevent *de novo* formation of metastases in a curative protocol. Our observations are in line with administration of an α_v integrin antagonist in breast cancer cells, which resulted in decreased tumor growth and bone metastasis in preclinical models of breast cancer [46].

In conclusion, both our *in vitro* data and our preclinical models show that administration of GLPG0187 inhibits multiple processes along the bone metastatic cascade. Targeting of integrins by GLPG0187 can inhibit the *de novo* formation and progression of bone metastases in prostate cancer by antitumor (including inhibition of EMT and the size of the prostate cancer stem/progenitor cell population), antiresorptive, and antiangiogenic mechanisms. GLPG0187 can therefore potentially be used to treat bone metastases in prostate cancer.

References

[1] Frydenberg M, Stricker PD, and Kaye KW (1997). Prostate cancer diagnosis and management. *Lancet* **349**, 1681–1687.

[2] van der Pluijm G (2010). Epithelial plasticity, cancer stem cells and bone metastasis formation. *Bone* **48**(1), 37–43.

[3] Kong D, Banerjee S, Ahmad A, Li Y, Wang Z, Sethi S, and Sarkar FH (2010). Epithelial to mesenchymal transition is mechanistically linked with stem cell signatures in prostate cancer cells. *PLoS One* **5**, e12445.

[4] van den Hoogen C, van der Horst G, Cheung H, Buijs JT, Lippitt JM, Guzman-Ramirez N, Hamdy FC, Eaton CL, Thalmann GN, Cecchini MG, et al. (2010). High aldehyde dehydrogenase activity identifies tumor-initiating and metastasis-initiating cells in human prostate cancer. *Cancer Res* **70**, 5163–5173.

[5] Kelly K and Yin JJ (2008). Prostate cancer and metastasis initiating stem cells. *Cell Res* **18**, 528–537.

[6] Fornaro M, Manes T, and Languino LR (2001). Integrins and prostate cancer metastases. *Cancer Metastasis Rev* **20**, 321–331.

[7] Felding-Habermann B (2003). Integrin adhesion receptors in tumor metastasis. *Clin Exp Metastasis* **20**, 203–213.

[8] Hood JD and Cheresh DA (2002). Role of integrins in cell invasion and migration. *Nat Rev Cancer* **2**, 91–100.

[9] Brooks PC, Clark RA, and Cheresh DA (1994). Requirement of vascular integrin $\alpha_v\beta_3$ for angiogenesis. *Science* **264**, 569–571.

[10] Nakamura I, Duong IT, Rodan SB, and Rodan GA (2007). Involvement of $\alpha_v\beta_3$ integrins in osteoclast function. *J Bone Miner Metab* **25**, 337–344.

[11] Parise LV, Lee J, and Juliano RL (2000). New aspects of integrin signaling in cancer. *Semin Cancer Biol* **10**, 407–414.

[12] Tantivejkul K, Kalikin LM, and Pienta KJ (2004). Dynamic process of prostate cancer metastasis to bone. *J Cell Biochem* **91**, 706–717.

[13] Moschos SJ, Drogowski LM, Reppert SL, and Kirkwood JM (2007). Integrins and cancer. *Oncology (Williston Park)* **21**, 13–20.

[14] Ren B, Yu YP, Tseng GC, Wu C, Chen K, Rao UN, Nelson J, Michalopoulos GK, and Luo JH (2007). Analysis of integrin α_7 mutations in prostate cancer, liver cancer, glioblastoma multiforme, and leiomyosarcoma. *J Natl Cancer Inst* **99**, 868–880.

[15] Bonkhoff H, Stein U, and Remberger K (1993). Differential expression of α_6 and α_2 very late antigen integrins in the normal, hyperplastic, and neoplastic prostate: simultaneous demonstration of cell surface receptors and their extracellular ligands. *Hum Pathol* **24**, 243–248.

[16] King TE, Pawar SC, Majuta L, Sroka IC, Wynn D, Demetriou MC, Nagle RB, Porreca F, and Cress AE (2008). The role of α_6 integrin in prostate cancer migration and bone pain in a novel xenograft model. *PLoS One* **3**, e3535.

[17] Zhang X, Fournier MV, Ware JL, Bissell MJ, Yacoub A, and Zehner ZE (2009). Inhibition of vimentin or β_1 integrin reverts morphology of prostate tumor cells grown in laminin-rich extracellular matrix gels and reduces tumor growth *in vivo*. *Mol Cancer Ther* **8**, 499–508.

[18] Nagle RB, Knox JD, Wolf C, Bowden GT, and Cress AE (1994). Adhesion molecules, extracellular matrix, and proteases in prostate carcinoma. *J Cell Biochem Suppl* **19**, 232–237.

[19] Zheng DQ, Woodard AS, Fornaro M, Tallini G, and Languino LR (1999). Prostatic carcinoma cell migration via $\alpha_v\beta_3$ integrin is modulated by a focal adhesion kinase pathway. *Cancer Res* **59**, 1655–1664.

[20] Birnie R, Bryce SD, Roome C, Dussupt V, Droop A, Lang SH, Berry PA, Hyde CF, Lewis JL, Stower MJ, et al. (2008). Gene expression profiling of human prostate cancer stem cells reveals a pro-inflammatory phenotype and the importance of extracellular matrix interactions. *Genome Biol* **9**, R83.

[21] Park CC, Zhang H, Pallavicini M, Gray JW, Baehner F, Park CJ, and Bissell MJ (2006). β_1 Integrin inhibitory antibody induces apoptosis of breast cancer cells, inhibits growth, and distinguishes malignant from normal phenotype in three dimensional cultures and *in vivo*. *Cancer Res* **66**, 1526–1535.

[22] Van Aarsen LA, Leone DR, Ho S, Dolinski BM, McCoon PE, LePage DJ, Kelly R, Heaney G, Rayhorn P, Reid C, et al. (2008). Antibody-mediated blockade of integrin $\alpha_v\beta_6$ inhibits tumor progression *in vivo* by a transforming growth factor-β–regulated mechanism. *Cancer Res* **68**, 561–570.

[23] Bisanz K, Yu J, Edlund M, Spohn B, Hung MC, Chung LW, and Hsieh CL (2005). Targeting ECM-integrin interaction with liposome-encapsulated small interfering RNAs inhibits the growth of human prostate cancer in a bone xenograft imaging model. *Mol Ther* **12**, 634–643.

[24] McCabe NP, De S, Vasanji A, Brainard J, and Byzova TV (2007). Prostate cancer specific integrin $\alpha_v\beta_3$ modulates bone metastatic growth and tissue remodeling. *Oncogene* **26**, 6238–6243.

[25] Hynes RO (2007). Cell-matrix adhesion in vascular development. *J Thromb Haemost* **5**(suppl 1), 32–40.

[26] Nicholson B and Theodorescu D (2004). Angiogenesis and prostate cancer tumor growth. *J Cell Biochem* **91**, 125–150.

[27] Jimenez JA, Kao C, Raikwar S, and Gardner TA (2006). Current status of anti-angiogenesis therapy for prostate cancer. *Urol Oncol* **24**, 260–268.

[28] Sakamoto S, Ryan AJ, and Kyprianou N (2008). Targeting vasculature in urologic tumors: mechanistic and therapeutic significance. *J Cell Biochem* **103**, 691–708.

[29] Kim S, Bakre M, Yin H, and Varner JA (2002). Inhibition of endothelial cell survival and angiogenesis by proteinase A. *J Clin Invest* **110**, 933–941.

[30] Mahabeleshwar GH, Feng W, Phillips DR, and Byzova TV (2006). Integrin signaling is critical for pathological angiogenesis. *J Exp Med* **203**, 2495–2507.

[31] Sun LC, Luo J, Mackey LV, Fuselier JA, and Coy DH (2007). A conjugate of camptothecin and a somatostatin analog against prostate cancer cell invasion via a possible signaling pathway involving PI3K/Akt, $\alpha_V\beta_3/\alpha_V\beta_5$ and MMP-2/-9. *Cancer Lett* **246**, 157–166.

[32] Abdollahi A, Griggs DW, Zieher H, Roth A, Lipson KE, Saffrich R, Grone HJ, Hallahan DE, Reisfeld RA, Debus J, et al. (2005). Inhibition of $\alpha_v\beta_3$ integrin survival signaling enhances antiangiogenic and antitumor effects of radiotherapy. *Clin Cancer Res* **11**, 6270–6279.

[33] Buijs JT, Rentsch CA, van der Horst G, van Overveld PG, Wetterwald A, Schwaninger R, Henriquez NV, ten Dijke P, Borovecki F, Markwalder R, et al. (2007). BMP7, a putative regulator of epithelial homeostasis in the human prostate, is a potent inhibitor of prostate cancer bone metastasis *in vivo*. *Am J Pathol* **171**, 1047–1057.

[34] van der Horst G, van der Werf SM, Farih-Sips H, van Bezooijen RL, Lowik CW, and Karperien M (2005). Downregulation of Wnt signaling by increased expression of Dickkopf-1 and -2 is a prerequisite for late-stage osteoblast differentiation of KS483 cells. *J Bone Miner Res* **20**, 1867–1877.

[35] Petersen M, Pardali E, van der Horst G, Cheung H, van den Hoogen C, van der Pluijm G, and ten Dijke P (2010). Smad2 and Smad3 have opposing roles in breast cancer bone metastasis by differentially affecting tumor angiogenesis. *Oncogene* **29**, 1351–1361.

[36] Pfaffl MW (2001). A new mathematical model for relative quantification in real-time RT-PCR. *Nucleic Acids Res* **29**, e45.

[37] van der Pluijm G, Deckers M, Sijmons B, de Groot H, Bird J, Wills R, Papapoulos S, Baxter A, and Lowik C (2003). *In vitro* and *in vivo* endochondral bone formation models allow identification of anti-angiogenic compounds. *Am J Pathol* **163**, 157–163.

[38] Brabletz T, Jung A, Spaderna S, Hlubek F, and Kirchner T (2005). Opinion: migrating cancer stem cells—an integrated concept of malignant tumour progression. *Nat Rev Cancer* **5**, 744–749.

[39] Mani SA, Guo W, Liao MJ, Eaton EN, Ayyanan A, Zhou AY, Brooks M, Reinhard F, Zhang CC, Shipitsin M, et al. (2008). The epithelial-mesenchymal transition generates cells with properties of stem cells. *Cell* **133**, 704–715.

[40] Morel AP, Lievre M, Thomas C, Hinkal G, Ansieau S, and Puisieux A (2008). Generation of breast cancer stem cells through epithelial-mesenchymal transition. *PLoS One* **3**, e2888.

[41] Davies J, Warwick J, Totty N, Philp R, Helfrich M, and Horton M (1989). The osteoclast functional antigen, implicated in the regulation of bone resorption, is biochemically related to the vitronectin receptor. *J Cell Biol* **109**, 1817–1826.

[42] Ruoslahti E and Engvall E (1997). Integrins and vascular extracellular matrix assembly. *J Clin Invest* **99**, 1149–1152.

[43] Nieswandt B, Brakebusch C, Bergmeier W, Schulte V, Bouvard D, Mokhtari-Nejad R, Lindhout T, Heemskerk JW, Zirngibl H, and Fassler R (2001). Glycoprotein VI but not $\alpha_2\beta_1$ integrin is essential for platelet interaction with collagen. *EMBO J* **20**, 2120–2130.

[44] Jurdic P, Saltel F, Chabadel A, and Destaing O (2006). Podosome and sealing zone: specificity of the osteoclast model. *Eur J Cell Biol* **85**, 195–202.

[45] Pecheur I, Peyruchaud O, Serre CM, Guglielmi J, Voland C, Bourre F, Margue C, Cohen-Solal M, Buffet A, Kieffer N, et al. (2002). Integrin $\alpha_v\beta_3$ expression confers on tumor cells a greater propensity to metastasize to bone. *FASEB J* **16**, 1266–1268.

[46] Zhao Y, Bachelier R, Treilleux I, Pujuguet P, Peyruchaud O, Baron R, Clement-Lacroix P, and Clezardin P (2007). Tumor $\alpha_v\beta_3$ integrin is a therapeutic target for breast cancer bone metastases. *Cancer Res* **67**, 5821–5830.

[47] Thiery JP, Acloque H, Huang RY, and Nieto MA (2009). Epithelial-mesenchymal transitions in development and disease. *Cell* **139**, 871–890.

[48] Oft M, Heider KH, and Beug H (1998). TGFβ signaling is necessary for carcinoma cell invasiveness and metastasis. *Curr Biol* **8**, 1243–1252.

[49] Margadant C and Sonnenberg A (2010). Integrin-TGF-β crosstalk in fibrosis, cancer and wound healing. *EMBO Rep* **11**, 97–105.

Supplementary Methods

Cell Culture

The human osteotropic PC-3M-Pro4 prostate cancer cells were generated from PC-3 cells (ATCC no. CRL-1435) by injecting PC-3 cells into athymic mouse prostates and selecting for clones with increasing metastatic potential by several rounds of reinjecting cells from xenograft tumors back into the mouse prostate. PC-3M-Pro4 cells were stably transfected with a CMV promoter–driven mammalian expression vector containing *firefly*-luciferase (pcDNA3.1 CMV-ff-luc). One clone with high luciferase activity was selected with neomycin (800 μg/ml; Life Technologies, Basel, Switzerland) and successfully used for *in vivo* bioluminescent imaging as described previously (e.g., Buijs et al. [2007]. *Am J Pathol* **171**, 1047–1057; and van den Hoogen et al. [2010]. *Cancer Res* **70**, 5163–5173). The androgen-independent and metastatic C4-2B cells were maintained as described previously (Thalmann et al. [2000]. *Prostate* **44**, 91–103).

Proliferation Assay

Cells were seeded at a density of 2500/cm^2 and allowed to grow overnight before treatment and then for an additional 1 to 3 days. Twenty microliters of MTS was added to the medium, and mitochondrial activity was measured at 490 nm after 2 hours of incubation at 37°C (CellTiter96 AQueous Non-Radioactive Cell proliferation assay; Promega, Madison, WI).

Apoptosis Assay

For apoptotic analysis, harvested cells were stained with AnnexinV/PI (Alexa Fluor 488 annexin V/Dead Cell Apoptosis Kit; Invitrogen), incubated for 15 minutes according to the manufacturer's protocol. Samples were analyzed with FACSCalibur2 (Becton Dickinson) and FCS Express software (De Novo).

Solid-Phase Assays

Integrins. Integrin $\alpha_2\beta_1$ was purified from detergent extracts of HT1080 fibrosarcoma cells as previously described [1]. Recombinant integrin $\alpha_4\beta_7$ was purchased from R&D Systems (Oxford, UK). Recombinant integrin $\alpha_5\beta_1$ was made as an Fc fusion protein as described before [2]. Recombinant α_v integrins were made using a baculovirus expression system in insect cells [3]. Note that the recombinant proteins contain the complete extracellular domains of the integrin.

Ligands. Rat tail tendon collagen was obtained from Sigma-Aldrich (Poole, Dorset, UK) and biotinylated as described [1]. Recombinant murine MAdCAM-1 Fc fusion protein was made in COS cells [4]. A recombinant fragment of human fibronectin containing type III repeats 6 to 10 was produced and biotinylated as described [5]. Purified human vitronectin was obtained from Sigma-Aldrich. Recombinant human latency-associated protein was purchased from R&D Systems and biotinylated using sulfo-NHS-LC-biotin (Pierce, Rockford, IL) according to the manufacturer's protocols.

General assay methods. For solid-phase assays, the binding of ligands to integrins was measured in the presence of 1 mM Mn^{2+} to activate the receptors. In brief, 96-well plates (Costar 12-area EIA/RIA; Corning Science Products, High Wycombe, UK) were coated with integrins (1-5 μg/ml in Dulbecco PBS) overnight at room temperature. Wells were then blocked for 2 hours with 200 μl of 5% (wt/vol) bovine serum albumin (BSA), 150 mM NaCl, 0.05% (wt/vol) NaN_3, and 25 mM Tris-HCl, pH 7.4 (blocking solution). The blocking solution was removed, and the wells were then washed three times with 200 μl of 150 mM NaCl, 25 mM Tris-HCl, and 1 mM $MnCl_2$, pH 7.4, containing 1 mg/ml BSA (buffer A). Ligands in buffer A were added to the wells in the absence or presence of inhibitors, and the plate was then incubated at room temperature for 2 hours. Unbound ligand was removed, and the wells were washed three times with buffer A. For biotinylated ligands, bound ligand was quantitated by addition of 1:500 dilution of ExtrAvidin peroxidase conjugate (Sigma-Aldrich) in buffer A for 30 minutes at room temperature (50 μl/well). For MAdCAM-Fc, bound ligand was quantitated by the addition of 1:1000 dilution of antihuman Fc peroxidase conjugate (Jackson, Suffolk, UK) 30 minutes at room temperature (50 μl/well). For vitronectin, bound ligand was quantitated by the addition of 1:500 dilution of antihuman vitronectin antibody VIT-2 (Sigma-Aldrich) for 30 minutes at room temperature followed by 1:1000 dilution of antihuman IgM peroxidase conjugate (Jackson) for 30 minutes at room temperature (50 μl/well). Wells were then washed four times with buffer A, and color was developed using ABTS substrate (50 μl/well; Pierce). Measurements obtained were the mean of four replicate wells. Background binding of ligands to wells coated with BSA alone was subtracted from all measurements. IC_{50} = concentration of inhibitor for 50% of maximal inhibition of ligand binding to the integrin used in the assay [6]. Data obtained were from a minimum of two experiments (n = 2 or n = 3).

ORX

Study design. The effect of GLPG0187 on bone loss was evaluated in 3-month-old castrated male mice after 4 weeks of treatment with dosing starting immediately after castration (preventive protocol). Two different modes of administration were used: either subcutaneous twice daily with 10, 30, or 100 mg/kg of GLPG0187, either oral, twice daily with 30, 100, or 300 mg/kg of GLPG0187.

Animal housing. Male BALB/c mice used were from Charles River Laboratories (l'Arbresle, France). Mice were 12 weeks old at the time of castration and were maintained under controlled and continuously monitored conditions of temperature (21 ± 2°C), humidity (45% ± 10%), photo period (12:12-hour light-dark), and air exchange. All animals were maintained on a diet and tap water *ad libitum*.

Orchidectomy procedure. Mice were injected intraperitoneally (i.p.) with anesthesia solution 100 μl/100 g BW (Kétamine; ImalgèneR 1000; Merial, Villeurbanne, France). Postoperative care: castrated mice were maintained in a wakeup room for 2 hours, on a cellulose bed under a warming lamp before being reinstalled in their homing room.

Bone measurements. Mice tibias were recovered from 16-week-old mice after sacrifice and were used for tomodensitometric, histomorphometric, and densitometric analyses.

Tomodensity. Left tibias were collected, fixed overnight in formalin, and then stored at 4°C in 70% ethanol for micro-CT scanning. Basic structural metrics were measured using direct two-dimensional morphometry (Micro-densitometer Scanco μCT20, Software version 1.6 update in 2006; Scanco Medical, Brüttisellen, Switzerland) Micro-CT

scans of the metaphyseal region were performed at an isotropic resolution of 9 μm to obtain trabecular bone structural parameters. The bone tissue was segmented from the marrow using a global threshold procedure. Using a two-dimensional model, bone volume, bone surface, and the trabecular thickness were determined. Cortical and trabecular bones were separated using a semiautomated contour-tracking algorithm to detect the outer and inner boundaries of the cortex [7,8].

References

[1] Clément-Lacroix P, Berrocal E, Heckmann B, Wigerinck P, Lorenzon G, and Pujuguet P (2011). GLPG0187 inhibits progression of established bone metastasis and achieves maximum efficacy when combined with standard-of-care metastatic breast cancer treatments. *Bone* **48**, S45.

[2] Tuckwell DS, Smith L, Korda M, Askari JA, Santoso S, Barnes MJ, Farndale RW, and Humphries MJ (2000). Monoclonal antibodies identify residues 199-216 of the integrin alpha$_2$ vWFA domain as a functionally important region within alpha$_2$beta$_1$. *Biochem J* **350**, 485–493.

[3] Humphries M (2008). Integrin antagonist specificity profiling. Study report BC#0016/Report GLPG0187-PD-003.

[4] Coe APF, Askari JA, Kline AD, Robinson MK, Kirby H, Stephens PE, and Humphries MJ (2001). Generation of a minimal alpha$_5$beta$_1$ integrin-Fc fragment. *J Biol Chem* **276**, 35854–35866.

[5] Mould AP, Askari JA, Aota S, Yamada KM, Irie A, Takada Y, Mardon HJ, and Humphries MJ (1997). Defining the topology of integrin alpha$_5$beta$_1$-fibronectin interactions using inhibitory anti-alpha$_5$ and anti-beta$_1$ monoclonal antibodies. Evidence that the synergy sequence of fibronectin is recognized by the amino-terminal repeats of the alpha$_5$ subunit. *J Biol Chem* **272**, 17283–17292.

[6] Mould AP, Koper EJ, Byron A, Zahn G, and Humphries MJ (2009). Mapping the ligand-binding pocket of integrin alpha$_5$beta$_1$ using a gain-of-function approach. *Biochem J* **424**, 179–189.

[7] Kapadia RD, Stroup GB, Badger AM, Koller B, Levin JM, Coatney RW, Dodds RA, Liang X, Lark MW, and Gowen M (1998). Applications of micro-CT and MR microscopy to study pre-clinical models of osteoporosis and osteoarthritis. *Technol Health Care* **6**(5–6), 361–372.

[8] Rüegsegger P, Koller B, and Müller R (1996). A microtomographic system for the nondestructive evaluation of bone architecture. *Calcif Tissue Int* **58**(1), 24–29.

Table W1. Real-time qPCR Primers.

Gene	5′ Sequence	3′ Sequence
Twist	TGTCCGCGTCCCACTAGC	TGTCCATTTTCTCCTTCTCTGGA
Snail1	TGCAGGACTCTAATCCAAGTTTACCC	GTGGGATGGCTGCCAGC
Snail2	TGTGTGGACTACCGCTGC	TCCGGAAAGAGGAGAGAGG
GAPDH	GACAGTCAGCCGCATCTTC	GCAACAATATCCACTTTACCAGAG

Exon-spanning real-time PCR primers designed with Primer Express software (Applied Biosystems, Rotkreuz, Switzerland).

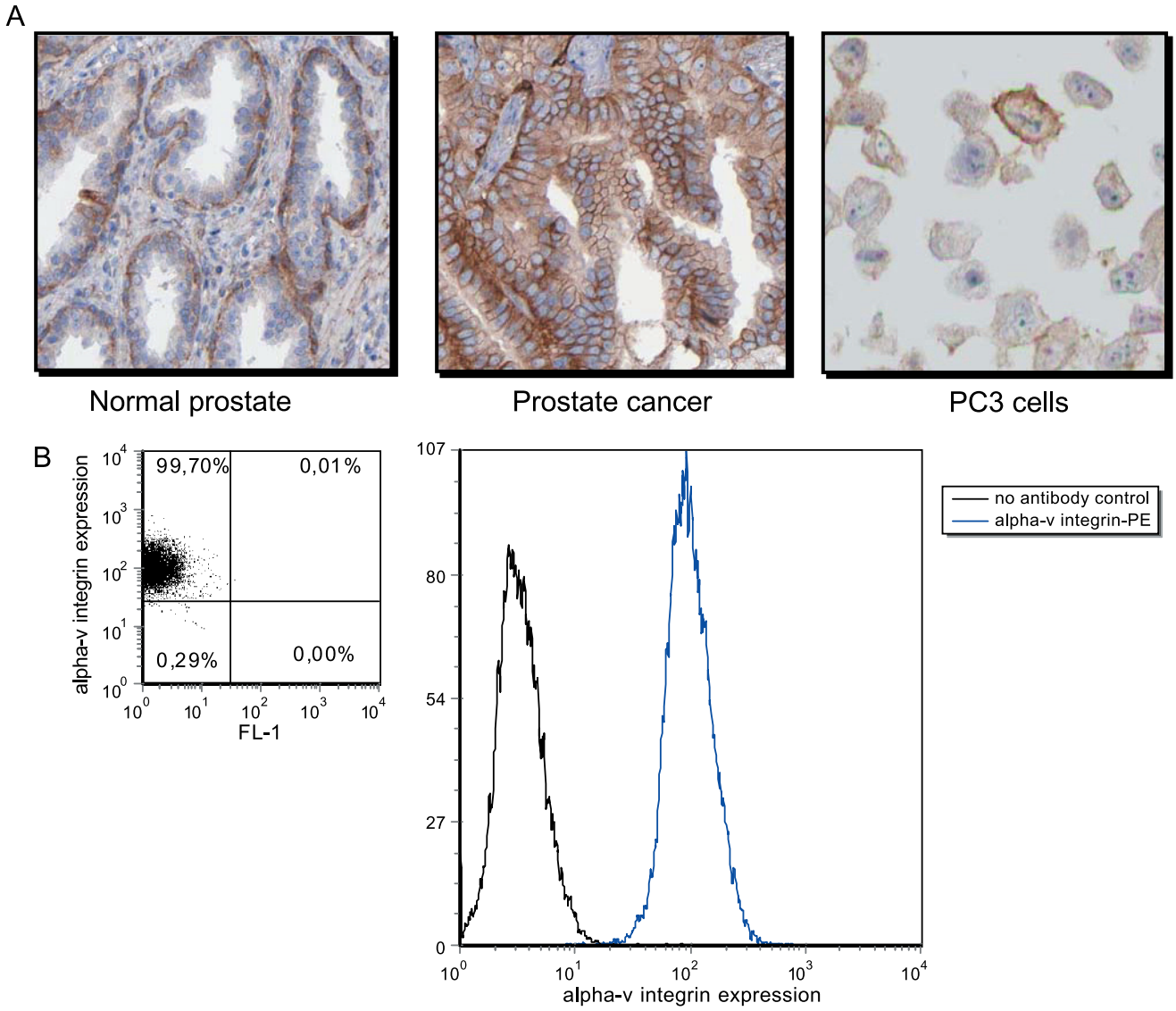

Figure W1. Immunolocalization and expression of α_v-integrin in normal prostate, prostate cancer tissue, and prostate cancer cell line. (A) Tissue sections of normal human prostate (left panel), human prostate carcinoma (middle panel), or the human prostate cancer cell line PC3 (right panel). Sections were stained with α_v-integrin antibody (Novocastra, Leica Microsystems BV, Rijswijk, The Netherlands; data source: protein atlas www.proteinatlas.org). (B) Dot plot and histogram showing integrin-α_v expression in PC-3M-Pro4/luc cells.

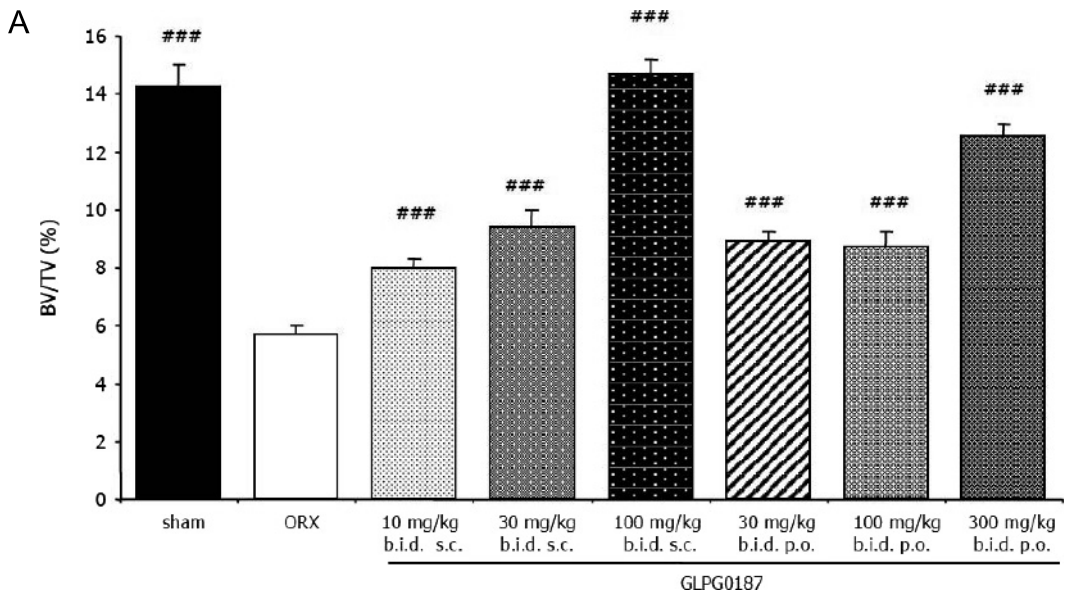

Figure W2. Effect of GLPG0187 (subcutaneously or orally) on trabecular bone volume loss in ORX mice assessed on proximal tibia metaphysis. (A) Three-month-old ORX male mice ($n = 8$) were treated for 4 weeks either with vehicle or with GLPG0187, with dosing initiated immediately after ORX. The effects on bone loss were monitored by measuring changes in trabecular bone volume (BV/TV). Data are expressed as mean ± SEM. $###P < .001$ *versus* ORX mice.

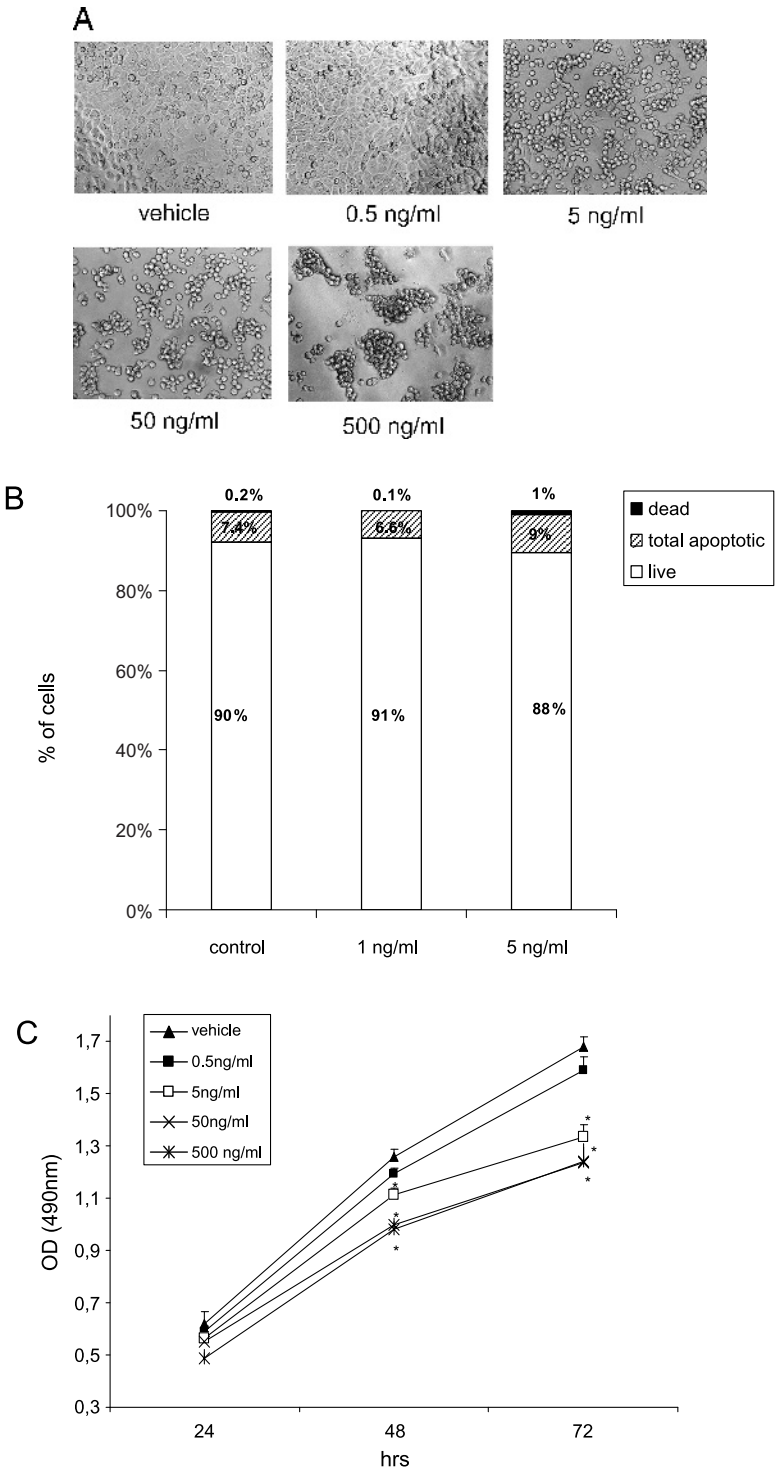

Figure W3. *In vitro* effects of GLPG0187 on proliferation and apoptosis. (A) Representative images of PC-3M-Pro4 cells treated with either vehicle or different concentrations of GLPG0187 for 24 hours. (B) PC-3M-Pro4 cells were seeded into a six-well plate and exposed to GLPG0187 (0, 1, and 5 ng/ml). At 48 hours after incubation, cells were harvested and processed for annexin V/PI staining with the Alexa Fluor 488 annexin V/Dead Cell Apoptosis Kit (Invitrogen). The percentage of live (AnnexinV−/PI−), dead (PI+/AnnexinV−), and total apoptotic cells (AnnexinV+) are shown. (C) Proliferation rate of PC-3M-Pro4/luc cells treated with either vehicle or GLPG0187 for 24, 48, and 72 hours was assessed with 3-(4,5-dimethylthiazol-2-yl)-2,5-diphenyltetrazolium bromide (optical density at 490 nm).

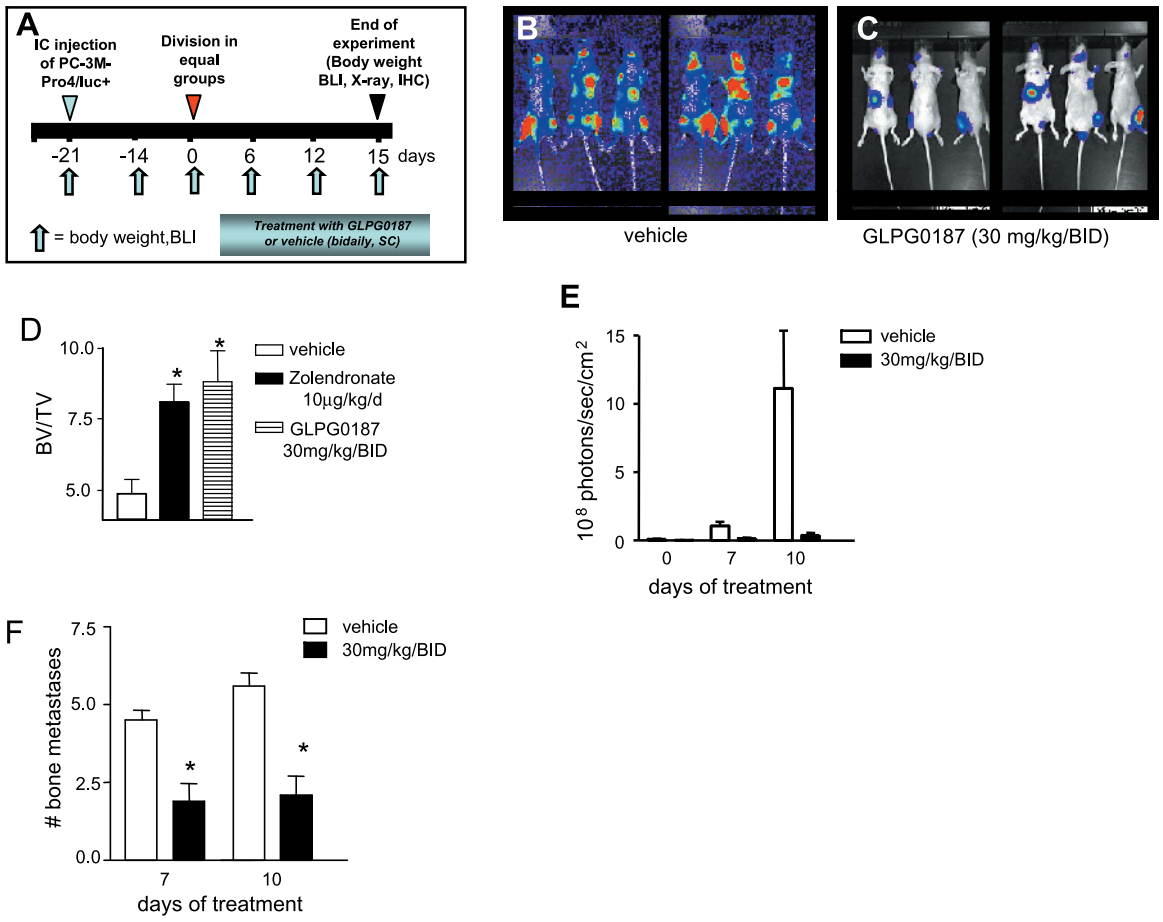

Figure W4. Effects of systemic administration (SC) of GLPG0187 on tumor growth of established (bone) metastases. (A) Schematic representation of the curative protocol. At day −21, 100,000 PC-3M-Pro4/luc cells were injected into the left heart ventricle, and once a week, body weight was measured, and BLI images were taken. At day 0, mice were divided into groups with equal total tumor burden. Mice were daily treated with either vehicle or GLPG0187 from day 0 onward. Representative images of mice treated with either vehicle (B) or 30-mg/kg per day GLPG0187 (C) taken at day 15 after start of treatment. (D) Ratio of bone volume (BV) over tumor volume (TV) of mice injected with vehicle, GLPG0187, or zoledronate (10 μg/kg per day) at day 15 of treatment. (E) Bone tumor burden for the mice treated with 30-mg/kg per day GLPG0187 (closed bars) or vehicle (open bars). (F) Total number of bone metastases per mouse (n = 10/group; *P < .05).

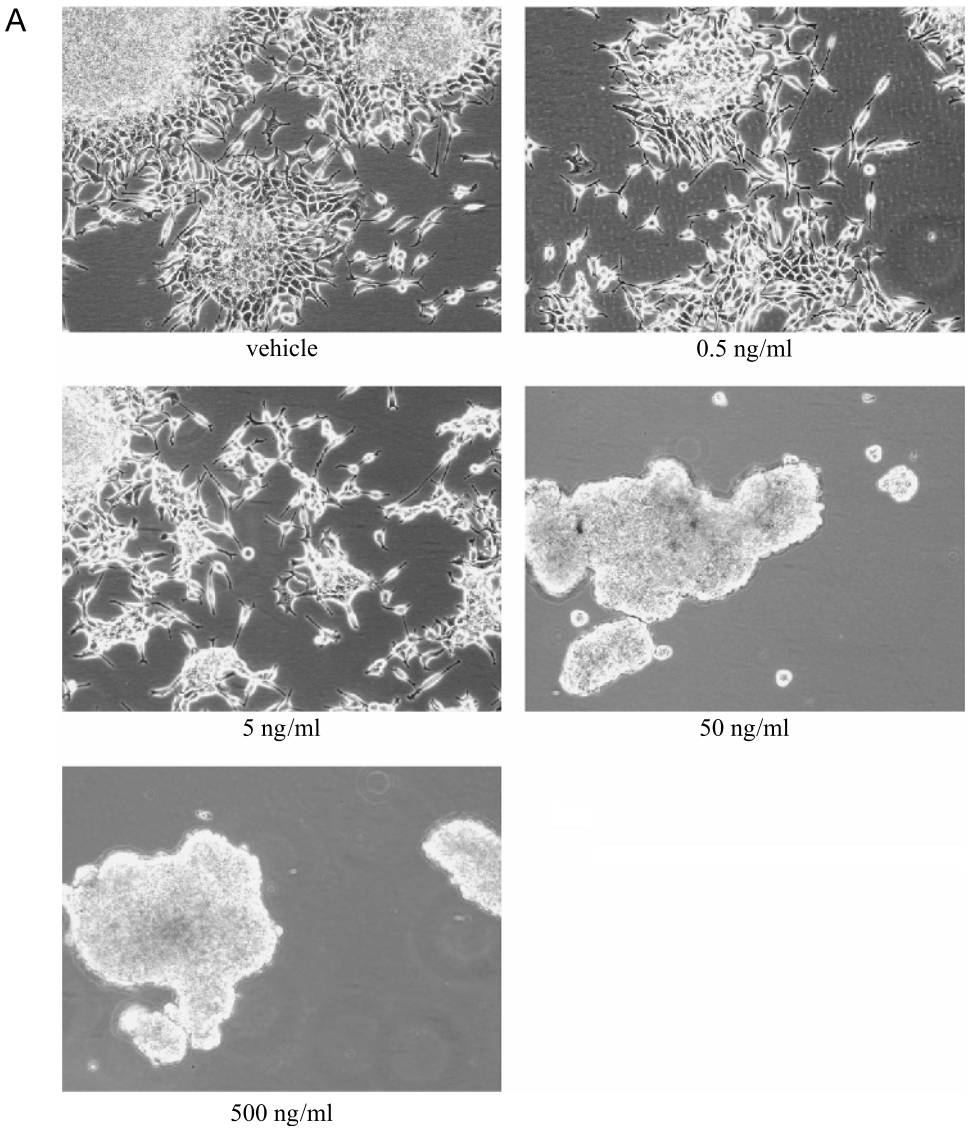

Figure W5. Effect of GLPG0187 on EMT, migration, and percentage of ALDH^{hi} stem/progenitor cells. (A) Representative images of C4-2B cells treated with either vehicle or different concentrations of GLPG0187 for 4 hours. (B) C4-2B cells were treated for 48 hours with a concentration range of GLPG0187, and subsequently, relative E-cadherin/vimentin ratio was measured with flow cytometry. (C) Percentage of C4-2B cells with high ALDH activity as measured with ALDEFLUOR assay. (D) Mean numbers of migrated C4-2B cells per field were measured. Data are presented as mean ± SEM (*$P < .05$) and are representative for two independent experiments.

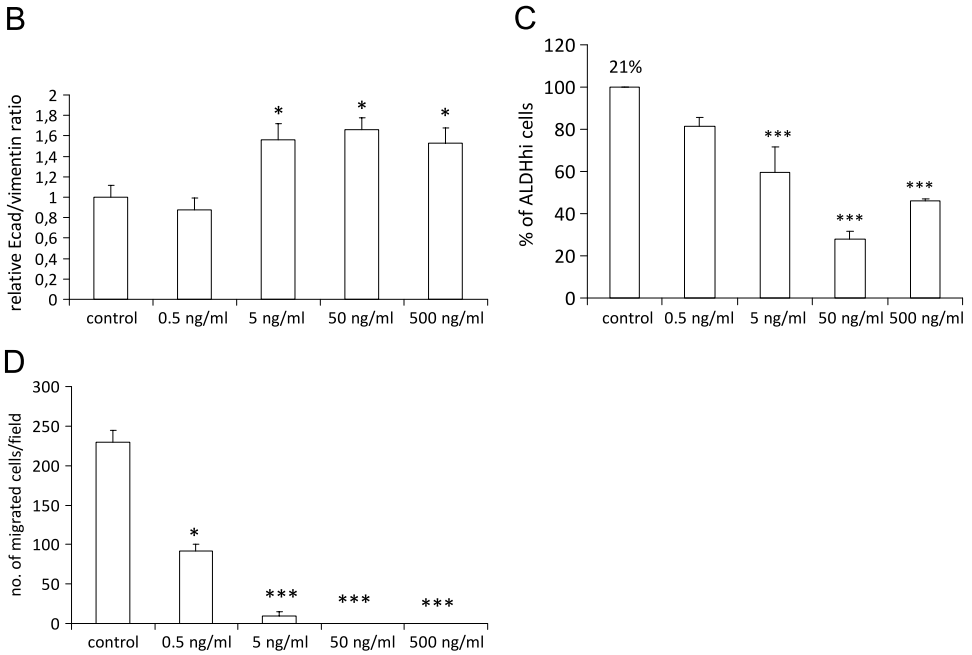

Figure W5. (*continued*).